EXTREME ULTRAVIOLET IMAGER OBSERVATIONS OF THE STRUCTURE AND DYNAMICS OF THE PLASMASPHERE

B. R. SANDEL
Lunar and Planetary Laboratory, The University of Arizona, Tucson, AZ 85721, USA

J. GOLDSTEIN
Department of Physics and Astronomy, Rice University, Houston, TX 77005, USA

D. L. GALLAGHER
National Space Science and Technology Center, NASA Marshall Space Flight Center, Huntsville, AL 35805, USA

M. SPASOJEVIC
STAR Lab, Stanford University, Stanford, CA 94305, USA

Abstract. The IMAGE Extreme Ultraviolet Imager (EUV) provides our first global images of the plasmasphere by imaging the distribution of He^+ in its 30.4-nm resonance line. The images reveal the details of a highly structured and dynamic entity. Comparing EUV images and selected *in-situ* observations has helped to validate the remote sensing measurements. The brightness in the EUV images is heavily weighted by the He^+ density near the plane of the magnetic equator, but two lines of evidence emphasize that the features seen by EUV extend far from the equator, and in at least some cases reach the ionosphere. Certain features and behaviors, including shoulders, channels, notches, and plasma erosion events, appear frequently in the EUV images. These are keys to understanding the ways that electric fields in the inner magnetosphere affect the large and meso-scale distribution of plasma, and their study can elucidate the mechanisms by which the solar wind and interplanetary magnetic field couple to the inner magnetosphere.

1. Introduction

The plasmasphere plays a central role in all processes in Earth's inner magnetosphere. After four decades of study by a variety of *in situ* and remote sensing (*e.g.*, whistler) techniques, we have a rather complete picture of some aspects of the formation and development of this important region. A simple theoretical formulation of the plasmasphere emerged rather early (Nishida, 1966; Brice, 1967). In this scenario, the configuration of the distribution of cold plasma in Earth's inner magnetosphere depends on the interplay between two electric fields, the corotation electric field and the convection electric field. The first of these, which enforces corotation of the cold plasma, dominates near Earth. The second electric field arises from the interaction between the solar wind and the magnetosphere, and is associated with the well-known sunward convection pattern. Where corotation is enforced, flux tubes are connected to the ionosphere for long periods. Cold plasma from the ionosphere can flow upward to populate these flux tubes, forming the

Space Science Reviews **109:** 25–46, 2003.

plasmasphere. In contrast, flux tubes outside the corotation region are continually carried toward the noon magnetopause and have little opportunity to become loaded with ionospheric plasma.

The first complication in this simple scenario arises because the strength of the convection electric field depends on solar wind conditions. When the convection electric field intensifies, the region where corotation is enforced shrinks, and the plasma moving along outer streamlines previously enclosing the dipole may be entrained by the convective flow. When the convection electric field diminishes, the corotation region expands to include some (now) depleted flux tubes, which can then refill from the ionosphere.

For many years we have known that this simple scenario, while correct in general, is incomplete, particularly with respect to processes occurring in what is becoming known as the plasmasphere boundary layer. Earlier observations have revealed a host of complex structures (*e.g.*, Horwitz *et al.*, 1990; Carpenter *et al.*, 2000). One of the chief goals of the IMAGE Extreme Ultraviolet Imager (EUV) is to provide global images, maps of plasma distributions that supply the context for *in situ* observations, both past and present. Here we summarize several investigations that illustrate this capability. We also show how global imaging of the plasma distribution has led to new types of investigation that were difficult or impossible with earlier techniques.

An example is the study by Burch *et al.* (2001b) showing that peak fluxes of energetic neutral atoms from the ring current overlap the plasmapause. Ring current loss processes including charge exchange, coulomb interactions, and wave-particle interactions are expected to peak in the regions of overlap (Jordanova *et al.*, 1997; Kozyra *et al.*, 1997; Fok *et al.*, 1991), leading to a strong loss of ring-current particles, but verification using *in situ* techniques was elusive. Simultaneous global imaging of the plasmasphere and ring current populations greatly simplified this kind of study. We discuss other examples in more detail in the following sections.

We introduce new terms for two features that are prominent in EUV images. Our aim is to avoid confusion by selecting names not currently used to describe other features of the plasmasphere or magnetosphere. These new terms are "notch" to replace "bite-out" and "void," and "channel" to replace "trough" in the sense described in Section 6. We call attention to these new names as they are introduced in the discussion that follows.

2. EUV Measurements

The EUV instrument images the distribution of cold He^+ in Earth's plasmasphere with a time resolution of 10 minutes and a spatial resolution of 0.1 R_E (at apogee) or better (Sandel *et al.*, 2001). The instrument consists of three wide-field cameras that are tuned to the 30.4-nm resonance line of He^+, which is excited in the plasmasphere by scattering of sunlight. The cameras' fields of view are offset

relative to one another (Sandel *et al.*, 2000). Images from the separate cameras are merged in ground processing to form a complete image. The flat-fielding correction is not perfect for all conditions, so darker vertical bands sometimes appear at the junctures between the cameras. Figure 1 shows an example EUV image. The sun is toward the lower right, and Earth's shadow extends through the plasmasphere in the opposite direction, toward the upper left. In this image auroral emission is prominent. EUV has some residual sensitivity longward of its target wavelength, extending to about 80 nm. It is likely that much of the auroral signal arises from the O^+ line at 53.9 nm (Burch *et al.*, 2001a). The bright horseshoe-shaped region extending out to about 1.25 R_E on the dayside comes from a combination of plasmaspheric He^+ 30.4-nm emission and ionospheric He 58.4-nm and O^+ 53.9-nm emissions. Well outside this area, the sharp drop to background intensity corresponds to the plasmapause. This image also illustrates three aspects of the plasmasphere that have proven especially accessible by EUV imaging techniques, a shoulder (lower center), a drainage plume (right), and a pre-midnight channel (top).

The brightness measured by EUV is proportional to the line integral of the He^+ abundance along lines of sight corresponding to each pixel in the image. Owing to the rapid drop in plasma density with increasing L, this integrated brightness is heavily weighted toward the minimum L along the line of sight. Figure 2 shows the cumulative He^+ 30.4-nm source function along a line of sight parallel to the magnetic dipole. To compute these curves, we assumed the equatorial He^+ abundance to follow the profile specified by Equation 4 of Gallagher *et al.* (2000), with a sharp cutoff simulating a plasmapause at $L = 5$. We took the abundance of He^+ along a field line to be constant, a condition that we expect to hold for $L > 2$, except under special circumstances. According to this plot, about half the light comes from a region within ± 0.5 R_E of the equatorial plane. More importantly, the bottom panel of the figure shows that about half the light comes from a narrow range of L that extends from the minimum value L_{min} to roughly $L_{min} + 0.12$. This range of L is comparable to the spatial resolution of EUV; therefore smearing in L as EUV integrates along the line of sight is limited to comfortable levels in the EUV images. Although Figure 2 was computed for lines of sight parallel to the dipole axis, the result shown in the bottom panel holds over a wide range of viewing conditions that encompasses all images used in work reported here.

We can use these properties of the plasma distribution to help remove the effects of changes in perspective that could otherwise affect the inferred size and shape of the plasmasphere, and the location of features within it (Roelof and Skinner, 2000). Most of the images in hand were acquired from relatively high magnetic latitude, *i.e.*, with lines of sight inclined at small to moderate angles to the magnetic dipole axis. For this observing geometry, we can partially correct perspective effects by mapping points in the image to the plane of the magnetic equator along magnetic field lines. The procedure that we use begins with a line of sight specified by choosing a particular pixel in an image. Using the known position of IMAGE relative to Earth, and the direction of the chosen line of sight, the mapping algorithm solves

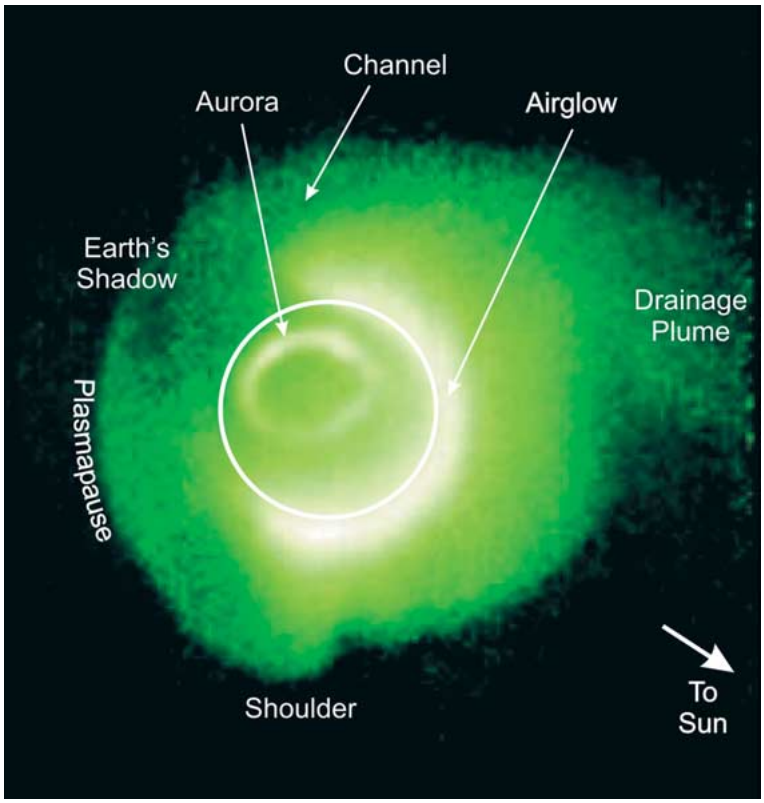

Figure 1. Extreme Ultraviolet Imager data at 07:34 UT on 24 May 2000, during a magnetic storm. A drainage plume extends sunward past the right edge of the image. Earth's shadow is visible in the direction away from the Sun, because only He^+ illuminated by the Sun scatters the target wavelength. The white circle shows the approximate size and position of Earth.

analytically to identify the dipole field line, among all those touching the line of sight, that has the minimum value of *L.* The algorithm reports the position of this field line in coordinates of *L* and magnetic longitude (or magnetic local time). In this paper, the plots that show projections of plasmaspheric features to the plane of the magnetic equator have been computed in this way.

3. Establishing the Context of Remote Sensing

For any remote sensing investigation, and especially for one carried out for the first time, it is appropriate to ask for independent confirmation that the remote observations are interpreted correctly. In the case of EUV, such testing against "ground-truth" has come from comparing with the results of two types of *in situ* observations. We discuss first a comprehensive comparison of the position of the plasmapause inferred independently from RPI and EUV observations.

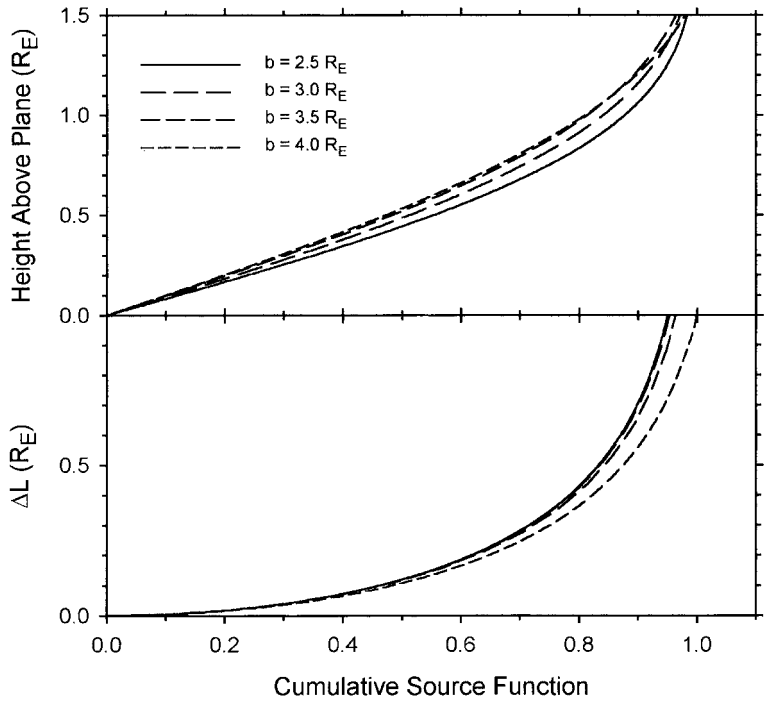

Figure 2. Integral source functions for EUV lines of sight that are parallel to the axis of the magnetic dipole. The parameter *b* is the distance of the line of sight from Earth's center. Top panel: Ordinate is distance from the plane of the magnetic equator. Bottom panel: Ordinate is the difference in *L*-values from the minimum *L* at the equator to the field point. The plotted quantity is the normalized line integral from the plane of the magnetic equator to the position specified by the ordinate. The plots tells us that, *e.g.*, about half the brightness seen by EUV under these conditions comes from the region within ± 0.5 R_E of the magnetic equator (top), and from a range of values of L from the minimum L_{min} to $L_{min} + 0.12$ (bottom).

3.1. Identifying the Plasmapause in EUV Images

In many EUV images, the He^+ 30.4-nm emission has a sharp outer boundary. It is natural to identify this edge with the plasmapause, but this identification should be tested quantitatively. The IMAGE Radio Plasma Imager, operated in its passive receiving mode, determines the local electron density along the trajectory of IMAGE, and hence can identify plasmapause crossings. Goldstein *et al.* (2002a) use this capability to demonstrate that the position of the plasmapause determined by RPI passive sounding usually coincides with the He^+ edge seen in EUV images.

They used data from the entire month of June 2001. For each orbit, they located the steep gradient in electron density that marked the plasmapause in RPI observations. Then they selected EUV images having the smallest available time difference, where possible both before and after the RPI measurement. From these images they extracted the location of the He^+ edge at the magnetic longitude

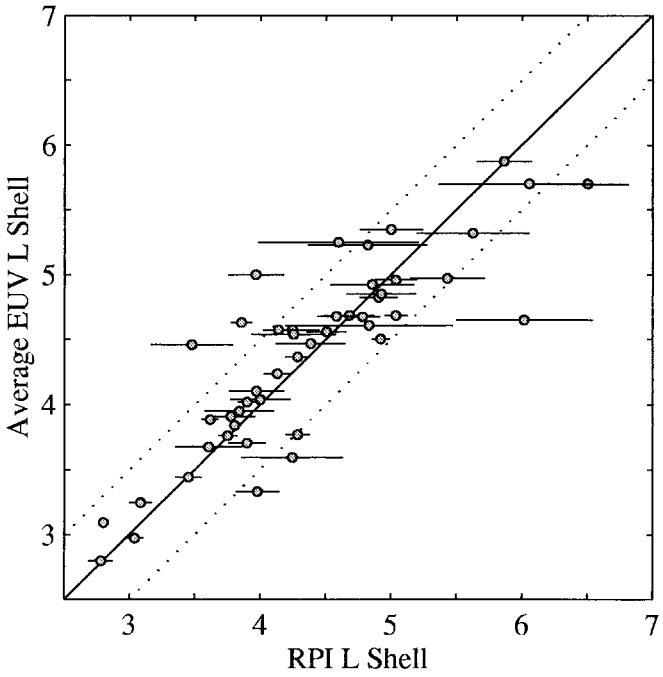

Figure 3. Comparison of the location of the plasmapause inferred from RPI observations with the position of the steep brightness gradient in EUV images. The correlation is 0.86, indicating good agreement between the methods. (From Goldstein *et al.*, 2002a).

corresponding to the RPI determination. They used only plasmapause crossings near dawn, owing to the possibility that corotation is less strictly enforced in the dusk sector (*e.g.*, Carpenter and Park, 1973). A breakdown in corotation could introduce errors, since extracting the plasmapause at the magnetic longitude of the RPI measurements implicitly assumes strict corotation of the plasma in the interval between EUV and RPI observations. Changes in position of the plasmapause owing to erosion or refilling between times of the *in situ* and remote measurements could be compensated only imperfectly in this analysis. Nevertheless, Goldstein *et al.* found excellent agreement between the positions of the plasmapause inferred from RPI measurements and the positions of the He^+ edge inferred from EUV images.

Figure 3 shows the correlation between these two positions found by Goldstein *et al.* The ordinate in this plot is the average of two remote determinations of the position of the He^+ edge, one from before and one after the RPI measurement, when both times are available. For orbits having only one EUV determination available, that value is used for the ordinate. For perfect agreement between the two techniques, all the points would fall on the diagonal line of slope unity. In fact, we see that there are significant departures from that line in some cases. However, 55% of the 47 points lie within 0.25 R_E of the line, and 81% lie within 0.5 R_E of it.

Therefore most of the points fall close enough to the line to indicate that the He^+ edge is a reliable proxy for the plasmapause.

Goldstein *et al.* discuss in more detail the reasons for some of the deviations from the ideal line. Of particular interest are the points marked by the larger horizontal error bars in Figure 3. The length of the horizontal bar is inversely proportional to $\mathrm{d}\log(n_e)/\mathrm{d}L$, that is, to the steepness of the gradient in electron density measured by RPI. The figure shows that most of the outlier points correspond to times having a shallow gradient, *i.e.*, to a diffuse, rather than a sharp, plasmapause. At such times, the position of the He^+ edge in EUV images can be quite uncertain.

3.2. Position Uncertainties and Detection Threshold

There is an unavoidable subjective aspect of our present technique for identifying boundaries in EUV images. As an adjunct to the study described above, two of the authors of Goldstein *et al.* each independently determined the positions of the He^+ edge for the complete set of images used. For 73% of the images, the two determinations agreed with 0.25 R_E. This figure may be compared with EUV's spatial resolution of 0.1 R_E at apogee. The cases for which the differences exceeded 0.25 R_E generally corresponded to diffuse, poorly defined He^+ edges.

Although such poorly defined edges with gradual fall-offs in intensity can lead to uncertainty in position determinations, they offer an advantage as well. Goldstein *et al.* have used measurements under these conditions to estimate the lowest value of n_e detectable by EUV. They call this value the lower sensitivity threshold, or LST. They identified the position in EUV images for which the plasmaspheric signal merged with the background, *i.e.*, was equal to the LST. They then determined the local electron density at that point from using RPI measurements. Their weighted average of 18 determinations gives a value of 40 ± 10 electrons cm^{-3} for the LST.

The meaning of this value should be clarified. Firstly, EUV measures a column abundance of He^+ ions rather than a local electron density. Therefore the distribution of He^+ along the line of sight and the ratio $n(He^+)/n_e$ both play a role in establishing the LST. Nevertheless, Goldstein *et al.* showed that an estimate of the LST made using the EUV sensitivity, measured background levels, a typical profile of He^+ ion concentration vs. L, and viewpoint at high latitude was consistent with the value determined by comparing EUV and RPI measurements. Finally, Moldwin *et al.* (this issue) have found a similar value by comparing EUV images with plasma measurements from the LANL geosynchronous satellites. Therefore we believe that this value of the LST represents a useful rule of thumb that is helpful in interpreting EUV images.

3.3. Comparison with Measurements at Geosynchronous Orbit

Moldwin *et al.* (2002, this issue) have undertaken a second comparison between EUV images and *in situ* observations, using the plasma density measurements of

the MPA instruments on the LANL geosynchronous satellites. Because this paper is in the same issue, we discuss it only briefly here. Moldwin *et al.* studied two time periods, an active time (24–25 May 2000) and a quiet time (2 May 2001). The main motivation for this study was to quantify the interpretation of EUV images by means of comparison with the *in situ* results. A useful by-product was a better understanding of the ways that remote (EUV) and *in situ* observations can complement one another.

The storm-time plasmasphere that they studied included a drainage plume extending sunward from the dusk region of the plasmasphere, and past the geosynchronous orbit. The drainage plume was also detected by the MPA instruments, which found its position and shape to be consistent with those inferred from the EUV images.

The quiet-time plasmasphere was quite extended, with a diffuse boundary. The most important question posed for this period concerned the consistency in the locations of the plasmapause inferred from the two sets of data. The *in situ* observations came from three regions of local time, roughly 2–4 hours, 8–10 hours, and 20–22 hours MLT. For this time period, the EUV images showed a dusk-side bulge in the plasmasphere that extended beyond geosynchronous orbit. The *in situ* results were entirely consistent with this conclusion (see Figure 10 of Moldwin *et al.* (2002)).

Moldwin *et al.* also were able to derive an independent value for the LST derived earlier. By comparing radial profiles of EUV intensity with *in situ* plasma density, they found a value of 30 to 40 electrons cm^{-3}, in good agreement with the values inferred by Goldstein *et al.*

4. Plasma Extends to High Latitudes

During the first two years of the IMAGE mission, most EUV observations have been from high latitudes. As the orbit's line of apsides precesses so that perigee is nearer the equator, EUV will have a more favorable viewpoint for studying the distribution of plasma out of the equatorial plane. However, for the observations in hand, the measured intensity is dominated by the He^+ distribution near the plane of the magnetic equator in the way described in Section 2. In this circumstance, EUV by itself tells us little about the distribution of plasma in the dimension perpendicular to the plane of the magnetic equator. Fortunately, combining EUV observations with other sources of information can fill this gap. In this section we discuss two such investigations, both of which show that plasmaspheric drainage plumes extend far out of the plane of the magnetic equator.

4.1. Drainage Plumes Map to the Ionosphere

Recent comparisons of maps of ionospheric total electron content (TEC) with EUV images show that plasmaspheric drainage plumes are manifest in the ionosphere, where they are related to storm enhanced density (SED). Therefore their effects must extend from the equatorial plane, where they are measured by EUV, all the way to Earth's upper atmosphere. For this work Foster *et al.* (2002) used maps of the vertical ionospheric TEC inferred from GPS measurements during the storm of 31 March 2001. Their map for 21:30 UT on 31 March 2001 (Figure 4) shows a pronounced band of SED extending diagonally across Canada and the northeastern United States from northwest to southeast. The red line shows the 50 TECu contour and outlines the main effects in the ionosphere.

In Figure 5, Foster *et al.* have projected the 50 TECu contours into the plane of the magnetic equator using the approximation of a dipole field. The circles in the same figure mark the position of the plasmapause inferred from the contemporaneous EUV image and mapped using the procedure described in Section 2. This figure illustrates the spatial correspondence between the ionospheric plume and the plasmaspheric drainage plume seen by EUV. The same analysis procedure carried out for other times showed that the equatorial and ionospheric manifestations of the drainage event tracked each other in space. The ionospheric maps further confirm the validity of the plasmapause position inferred from the EUV observations. This is particularly noteworthy given the unusually small plasmasphere recorded by EUV at the height of the storm. This builds confidence that the small plasmasphere seen by EUV is in fact a consequence of an unusually intense episode of plasmaspheric erosion, rather than an unexpected instrumental artifact.

4.2. Drainage Plumes at Mid-Latitudes

Comparisons of EUV and RPI measurements have identified a number of discrete regions of high electron density, far from the plane of the magnetic equator, that lay on the same geomagnetic field line as a drainage plume. Garcia *et al.* (2002) used RPI in its passive receiving mode to determine the local electron density along the IMAGE trajectory. Green and Reinisch (this issue) also discuss this investigation. Garcia *et al.* found a number of examples of "detached plasma regions" outside the main plasmasphere. Such regions have long been discussed in the literature, but Garcia *et al.* focused on a study of the relationship between such regions and drainage plumes as seen by EUV.

The EUV and RPI observations were not precisely contemporaneous, because the EUV images were acquired near apogee and the RPI *in situ* determinations were made a few hours earlier (for those made in the ascending portion of the orbit) or later (for the descending portion). Therefore it was important to understand the motion of the plume in the interval of time between the two measurements. Garcia *et al.* confined their attention to cases for which the plume structures were seen by EUV to be corotating or nearly so.

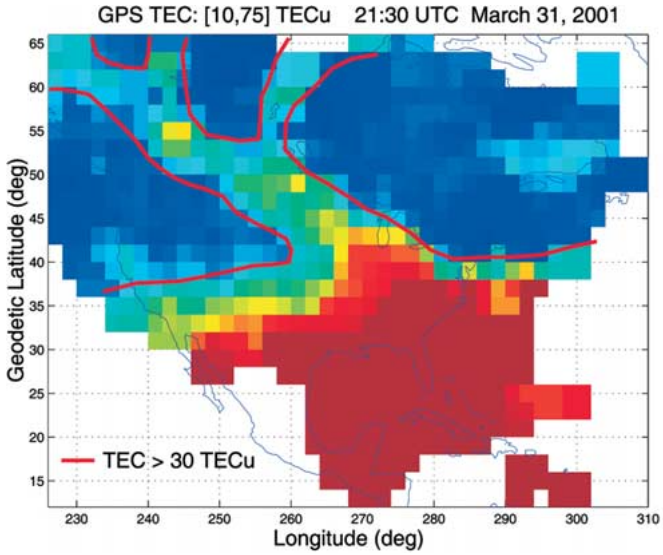

Figure 4. Map of total ionospheric electron content showing a plume of storm enhanced density (outlined in red). (From Foster *et al.*, 2002).

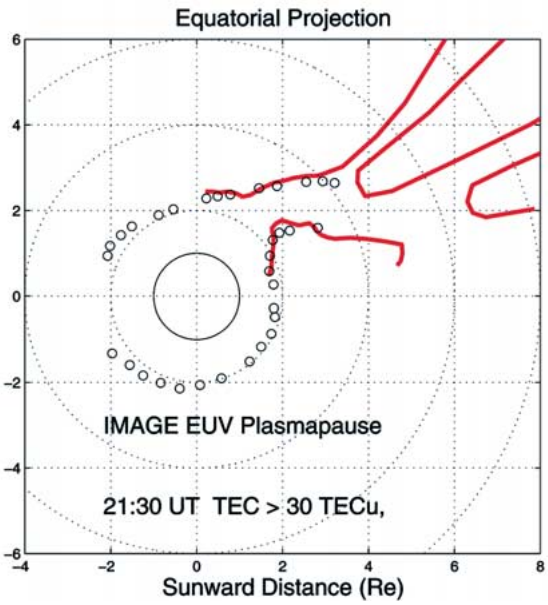

Figure 5. The red lines are the red boundaries from Figure 4 projected along dipole field lines to the plane of the magnetic equator. The circles show the position of the plasmapause at the same time determined from an EUV image. The drainage plume in the EUV image maps to the SED plume in the ionosphere. (From Foster *et al.*, 2002).

With this constraint, and using data that spanned 2001, Garcia *et al.* found eleven instances of excellent spatial correlation between "detached" regions and drainage plumes. Spatial correlation here means that both the "detached" region and the plume were threaded by common geomagnetic field lines, that is, lay on a common L-shell. The latitudes of the RPI measurements lay in the range from the equator to 38°. The electron densities found by RPI in the "detached" regions ranged from 11 to 2700 cm^{-3}.

Garcia *et al.* interpret their findings as evidence that the enhanced plasma density in the drainage plume is not confined near the plane of the magnetic equator, but extends along magnetic field lines to latitudes at least as high as 38°.

5. Structural Features of the Plasmasphere

Drainage plumes in the dusk sector are a common consequence of increased convection (Grebowsky, 1970; Carpenter *et al.*, 1992). We have discussed drainage plumes as seen by EUV in Section 4; Burch *et al.* (2001a, b) and *Sandel et al.* (2001) describe them from the point of view of EUV as well. EUV sees the plumes as narrow regions of enhanced density connected to the main body of the plasmasphere. As they form, the connection is in the dusk sector, and the plumes extend sunward. Typical size scales are 3–5 R_E in length and 0.5–1.0 R_E in width. The contrast over the gap separating the plume from the main plasmasphere is typically a factor of 5 in brightness (Sandel *et al.*, 2001), and often the region to the west of the plume is weakly enhanced in density even though it is far from the main plasmasphere. In the following section, we show how plumes may be related to the plasmaspheric channel, also shown in Figure 1.

An unexpected feature of the plasmasphere seen for the first time in EUV images is the "shoulder" (Burch *et al.*, 2001a, b), an asymmetric bulge in the plasmapause with a steep azimuthal gradient in He^+ density, usually toward earlier local times. Figure 1 shows an example. Burch *et al.* discussed a possible origin based on an association with a southward turning in the interplanetary magnetic field (IMF), and Section 9 describes further work on the origin of these structures.

Notches (previously called "voids" by Sandel *et al.* (2001) and "bite-outs" by Green *et al.* (2002)) are manifestations of localized low-density regions in the plasmasphere. A typical notch has an azimuthal extent of 5° to 20°, a radial extent of 1 to 2.5 R_E, and a brightness contrast of a factor of $\sim$3 against the main body of the plasmasphere. Most often, the region of lower density extends outward to the radial distance of the plasmapause inferred from the surrounding parts of the plasmasphere. Sections 7 and 8 show examples and relate them to physical processes in the plasmasphere.

From time to time, EUV images show that the plasmasphere shrinks rapidly. One cause of such inward motion of the plasmapause is the erosion expected in times of increasing magnetospheric convection, based on the simple picture de-

scribed in the Introduction. When convection returns to normal, flux tubes depleted by convection refill from the ionosphere. EUV observes the global effects of such events, but erosion, being the more rapid, is more dramatic and has been studied more thoroughly. Erosion occurs over at least the antisunward hemisphere, but not necessarily uniformly. The plasmapause may move at different times and at different rates at different local times. In Section 10, we show how this motion has been interpreted in terms of electric fields in the inner magnetosphere.

EUV images have shown many examples of the feature labeled "channel" in Figure 1, first discussed by Burch *et al*. (2001a, b) and called a "trough" by them. This is a region of lower density extending roughly in the azimuthal direction. Channels usually appear first in the pre-midnight sector, but sometimes extend from there through midnight and into the pre-dawn sector. In the following section we suggest a mechanism for forming channels.

Taken as a whole, the EUV observations emphasize the complexity in the structure of the plasmasphere on a wide range of length and time scales. Such complexity was expected on the basis of earlier work. Examples include investigations of the wide variety in the shape of radial density profiles (Horwitz *et al.*, 1990) and the presence of cavities (Carpenter *et al.*, 2000). Work is underway to understand the features appearing in the new global images in the context of these earlier investigations.

6. Drainage Plume Wraps to Form Channel

We have identified at least one mechanism that can create channels. The time sequence of images in Figure 6 illustrates how it works. The formation of the channel begins near the end of an erosion event in which a drainage plume has developed (left). Then, as convection decreases, corotation is re-established, first at values of L just outside the eroded plasmasphere. There the inner part of the plume begins to corotate while the outer parts remain strongly influenced by convective flow, and more nearly fixed in local time. In the middle panel of Figure 6 (four hours later), the base of the plume (nearer Earth) has corotated by about 60°. In this example, the base remains stationary near ∼225° magnetic longitude. The more distant parts of the plume are more nearly fixed in local time, so the plume begins to wrap around the plasmasphere. Nine hours later (right) the base of the plume has drifted westward in longitude, but only by about 15°, and the plume has wrapped so that its axis is roughly azimuthal. The low-density region between the plume and the main body of the plasmasphere has become the channel. Thus the channel represents yet another example of the interplay between corotation and convection electric fields.

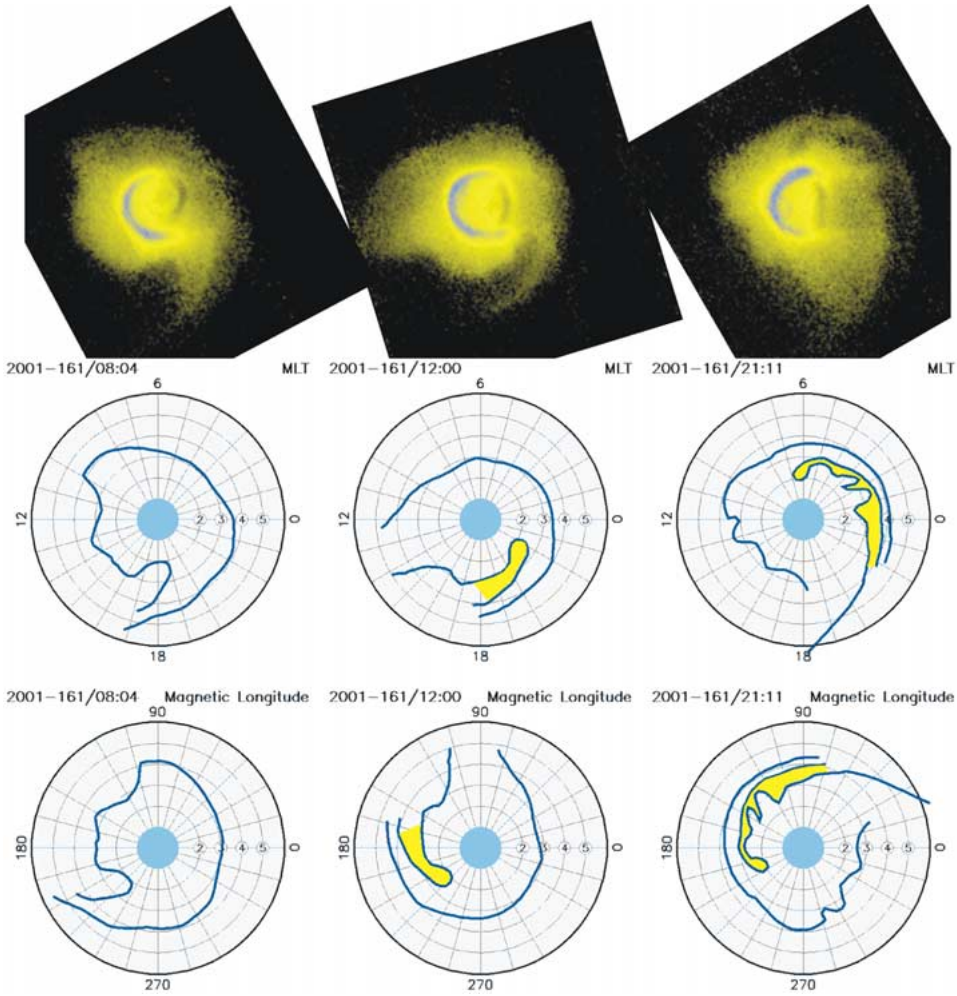

Figure 6. On day 2001-161, a channel formed in the pre-midnight sector when a drainage plume wrapped around the main body of the plasmasphere. After 13 hours, the leading edge of the channel reached the dawn meridian and the plume was wrapped around the anti-sunward hemisphere. Top row: EUV images, scaled to a common range and rotated so that the Sun is to the left. Middle row: Mapping of the prominent brightness gradients to the plane of the magnetic equator in [L, MLT] space. The yellow fill marks the channel. Bottom Row: As middle row, but in [L, magnetic longitude] space. The base of the plume remains nearly fixed near 225°, but the more distant parts of the plume are more nearly fixed in local time, so that the plume wraps to form a channel.

7. Kilometric Continuum Radiation and Notches

Work on the kilometric continuum radio emission by Green *et al.* (2002) (and also discussed by Green and Reinisch (this issue)) provides a further example showing how EUV imaging provides a valuable context for *in situ* observations, thereby enriching their interpretation. Kilometric continuum radio emission is a compon-

ent of the "escaping" non-thermal radio emission from Earth. It has recently been studied using data from the Plasma Wave instrument on Geotail (Hashimoto *et al.*, 1999). The component appears at all local times, is confined in latitude near the magnetic equator, and is localized in longitude.

Green *et al.* used the capability of EUV to image the plasma distribution near the source region to reach a better understanding of the properties of the source. For a particular instance of kilometric continuum radiation, they showed that the source region lay deep within a "bite-out" (which we now call a notch) or low-density region within the plasmasphere. Figure 7 shows the notch as seen by EUV. Fortuitously, the trajectory of IMAGE carried it through the notch shortly after this image was taken. Using the shape of the plasma distribution inferred from the EUV image, and ray-tracing calculations, Green *et al.* demonstrated that the longitudinal beaming of the emission could arise from refraction of waves emitted isotropically in azimuth. The refraction is strong enough to provide the observed beaming in longitude. However, there is no analogous mechanism to account for the confinement in latitude, so Green *et al.* conclude that this aspect is probably a property of the emission source.

8. Notches and Corotation

In addition to their intrinsic interest and their association with the kilometric continuum radiation, low-density regions can serve as natural markers that we use to track the positions of discrete volume elements of plasma. The notches have been observed to persist for periods as long as 60 hours. When they are persistent, and when they are few enough in number that we can unambiguously identify a particular notch in images from several orbits, we can use the notches to determine the angular velocity of the cold plasma over a range of values of L.

First we consider the history of the notch already described in connection with the investigation of the continuum kilometric radiation by Green *et al.* It is the longest-lived seen to date, having persisted in recognizable (but variable) form for 60 hours. In the upper part of Figure 7 are the EUV image and a plot showing the position of the plasmapause in L and magnetic longitude coordinates at the same time. Two notches are present; here we focus on the one at about 7.5 hours MLT. The bottom panel of Figure 7 shows the magnetic longitude of this notch over a 60-hour period. If the plasma were in strict corotation with Earth's magnetic field, then its magnetic longitude would remain constant. In fact, it drifts toward lower longitude, *i.e.*, westward, which corresponds to an angular velocity that is less than the corotation velocity. In this case, the angular rate is nearly constant at about 90% of the corotation value.

In contrast, the notch in Figure 8 moved at a variable rate during its lifetime. This feature has been described by Sandel *et al.* (2001). (See their Figure 3.) It is an unusually large notch, and shows the characteristic "W" shape that often

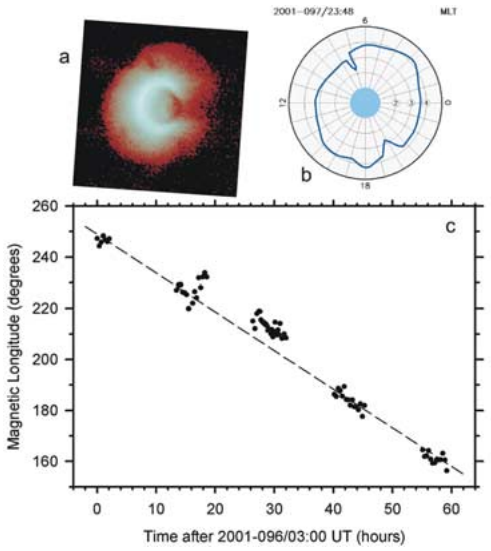

Figure 7. Example of a measurement of the angular velocity of plasmaspheric plasma. a) The EUV image for 23:48 UT on 7 April 2001, showing two notches separated by about 180° in azimuth. b) Mapping of prominent brightness gradients to the plane of the magnetic equator in [L, MLT] space. c) Magnetic longitude of the notch near 7.5 hours MLT in panel b as a function of time. Over this period of 60 hours, the notch drifted in longitude at a nearly constant rate. The dashed line corresponds to an angular velocity that is 90% of the corotation velocity.

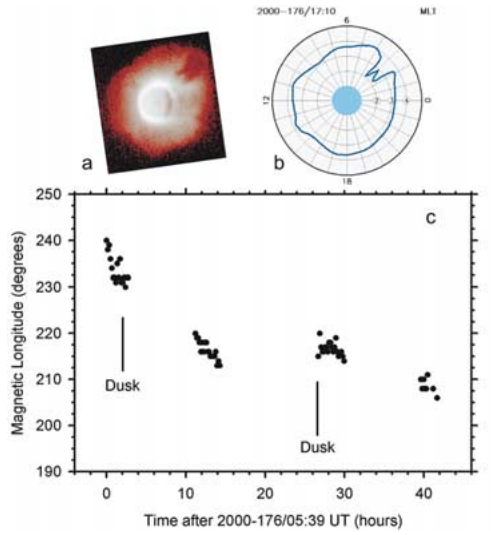

Figure 8. Same presentation as the previous figure, for a different time. a) Image for 17:12 UT on 24 June 2000. b) Mapping of prominent brightness gradients to the plane of the magnetic equator in [L, MLT] space. c) Longitude of the notch versus time. The notch drifted in longitude (again in the sense of rotating more slowly than the corotation rate), then remained fixed (corotated) for about 10 hours, and then returned to a sub-corotational drift.

TABLE I

Summary of angular velocity measurements for 13 features.

Property	Mean	Minimum	Maximum
Duration (hours)	31	15	60
Angular Rate Relative to Corotation*	0.88	0.77	0.93

*Averaged over the life of the feature. Some move at or near the corotation rate for part their lives.

appears in the larger notches. Figure 8a shows the EUV image, and Figure 8b is the mapping of the plasmapause to the plane of the magnetic equator at the same time. Figure 8c shows the position of the center of the notch in magnetic longitude. The notch moved rapidly between the apparitions near 0 hours and 10 hours, remained relatively stationary in longitude for the next ten hours, and then drifted slightly during the third 10-hour interval. The lines in the figure labeled "Dusk" mark the times at which the notch was at 18 MLT. Thus the pronounced drift in longitude between 0 and 10 hours occurred as the notch traversed the dusk and post-dusk sectors, the range of local times where departures from strict corotation might be most likely (Carpenter and Park, 1973). At other times, e.g., as in Figure 7, no local-time asymmetry in drift velocity is apparent.

We have identified 13 notches that persisted long enough to determine their angular rates. Table 1 summarizes the results of our analysis. Cold plasma in the range $2 < L < 4$ most frequently rotates at a rate that is roughly 85–90% of the corotation rate. A particular notch may move at a constant or variable rate during its lifetime. It may move at the corotation velocity for a time, and then begin to lag, as in the example discussed above.

Notches having substantial radial extent frequently maintain their shapes for many hours. In these cases, measurable shearing by an L-dependent corotation lag must therefore be absent.

9. Shoulder Formation

Section 5 briefly discussed the plasmaspheric shoulder shown in Figure 1. Goldstein *et al.* (2002b) have developed an explanation for this phenomenon based on the idea of a dusk-to-dawn overshielding electric field. They have used the Rice Magnetospheric Specification Model (MSM) (Freeman *et al.*, 1993; Wolf *et al.*, 1997) to quantify the concept. In their view, a pair of sudden northward turnings in the IMF triggered the formation of the shoulder by inducing an "overshielding" condition. Electric fields form at the earthward edge of the plasmasheet to counteract the effects of solar wind driven convection, thus shielding the inner magnetosphere from externally-imposed electric fields (Jaggi and Wolf, 1973).

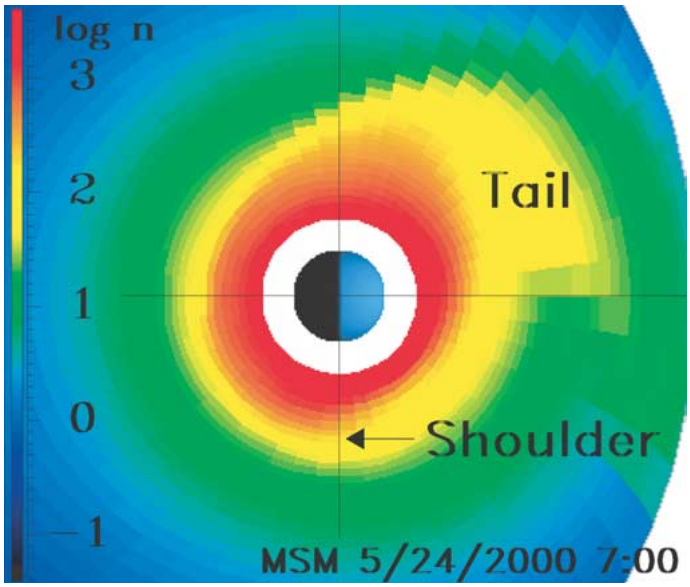

Figure 9. Simulation of the plasmasphere computed by the MSM. The shoulder and tail seen in EUV images from the same time are well reproduced by this model. The plotted quantity is the logarithm of the electron density. The Sun is to the right. (From Goldstein *et al.*, 2002b).

The IMF configuration after the northward turnings resulted in weaker magnetospheric convection, and hence a tendency toward change in the shielding field. However, the time constant for adjusting the shielding electric field is finite, leading to overshielding. That is, a field, called a penetration electric field, can persist in the inner magnetosphere, in this case from dusk to dawn.

This electric field leads to characteristic flow pattern in a pre-dawn "active region" where the plasma flow is predominantly outward, leading to a bulge in the plasmapause – the shoulder. On the other hand, a stagnation region near the dawn meridian suppresses outward motion there, and hence gives the shoulder its characteristic asymmetric shape. Figure 9 shows the results of the MSM simulation of the plasmasphere for a time 34 minutes prior to the image in Figure 1. The simulation reproduces the shoulder and drainage tail. The good agreement between this model and EUV images, coupled with the fact that shoulder formation has followed other northward turnings of the IMF, suggest that the ideas incorporated in the model are plausible.

10. Erosion of the Plasmasphere

The concept of erosion of the plasmasphere in times of intensified magnetospheric convection is central to our understanding of the inner magnetosphere (Section 1). Global imaging can elucidate the details of the erosion process in a way that

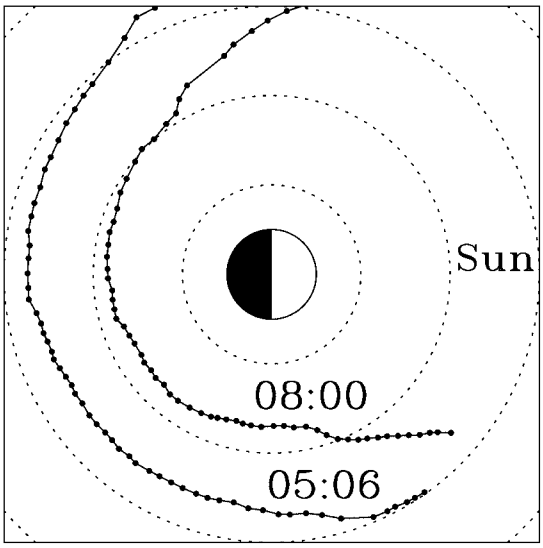

Figure 10. Erosion event of 10 July 2000. The dotted circles mark distances of 2, 4, and 6 R_E. The circles show the position of the plasmapause inferred from EUV image at two times about 3 hours apart. During the interval between these measurements, the plasmasphere was eroded, causing an inward displacement of the plasmapause by almost 2 R_E. (From Goldstein *et al.*, 2002c).

permits quantitative correlations with other measures of the strength of convection and the coupling between the solar wind and the inner magnetosphere. Such an investigation has been undertaken by Goldstein *et al.* (2002c), who studied an erosion event on 10 July 2000, between 04:24 and 09:32 UT. Figure 10 shows the position of the nightside plasmapause at two times separated by about 3 hours. In the interval between these measurements, the plasmapause moved inward by almost 2 R_E. Radial brightness profiles show either a decrease or constant brightness almost everywhere, so the change in plasmapause position must have been due to erosion, rather than to a global compression.

Goldstein *et al.* measured the plasmapause positions at 2.4 hours MLT for 31 times on ∼10-minute centers in the interval mentioned above, and compared the inferred motion of the plasmapause with z-component of the IMF and solar wind parameters measured by the Geotail satellite. To search for a correlation between plasmapause motion and IMF, Goldstein converted both quantities to parameters having units of electric field strength. These were, for the plasmapause position, $V_{pp}B_{dip}$, where V_{pp} is the measured velocity of the shrinking plasmapause at 2.4 hours MLT, and B_{dip} is the equatorial dipole field strength. For the IMF/solar wind, they used the quantity $V_{sw}B_z$, where V_{sw} is the solar wind velocity and B_z is the z-component of the IMF.

Figure 11 shows that these two parameters are well correlated with one another. In this plot, the IMF parameter has been delayed by 3.7 minutes (to account for the propagation time from Geotail) and an additional 30 minutes to achieve the

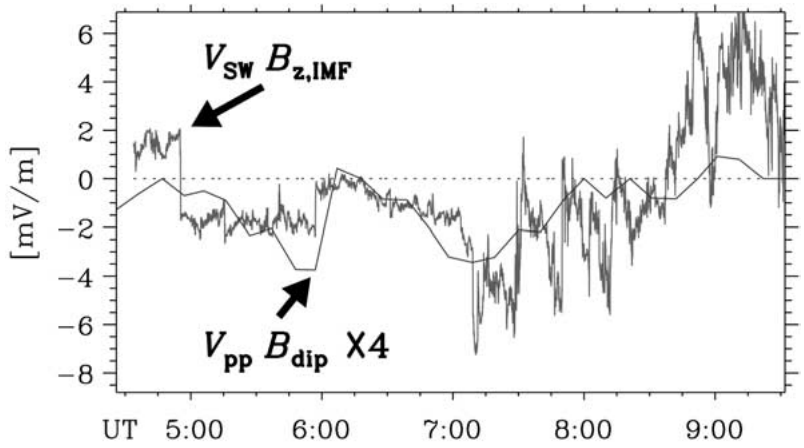

Figure 11. Comparison of the quantity $V_{pp}B_{dip}$ during the erosion event shown in Figure 10 with the $V_{sw}B_z$. The latter has been delayed by a response time constant of 30 minutes for the best correlation. (From Goldstein *et al.*, 2002c).

best correlation. The plot shows that there were two separate erosion events, one peaking at about 6 UT, and a second slightly more than an hour later. Both are associated with southward turnings of the IMF. Goldstein *et al.* point out that these close associations are consistent with the idea that the IMF polarity acts to switch on convection when it turns southward.

11. Image Inversion

EUV returns 2D images that represent a matrix of He^+ column densities along many lines of sight. An ideal goal is a 3D matrix of the plasmaspheric He^+ density, but an image from a single point of view contains insufficient information for a full 3D reconstruction. However, by assuming that the He^+ density is constant along a flux tube, one can invert the EUV images to produce He^+ density maps in the plane of the geomagnetic equator.

One approach to such an inversion uses an iterative technique (Gurgiolo *et al.* 2002, and C. Gurgiolo, personal communication). The inversion begins with an initial estimate of the He^+ density in the plane of the geomagnetic equator. The estimate is determined by assuming that the brightness in each pixel arises entirely from the minimum L value along the line of sight. This provides a base set of density as a function of both L and geomagnetic longitude, which is then mapped into a 3D solution matrix. Lines of sight that intersect Earth are excluded and lines of sight that intersect Earth's shadow are assigned the minimum L-shell outside the shadow region. The last step in the initialization is creating a simulated image using column densities computed from the solution matrix. The iterative procedure then compares simulated and real images. If the measured and simulated images

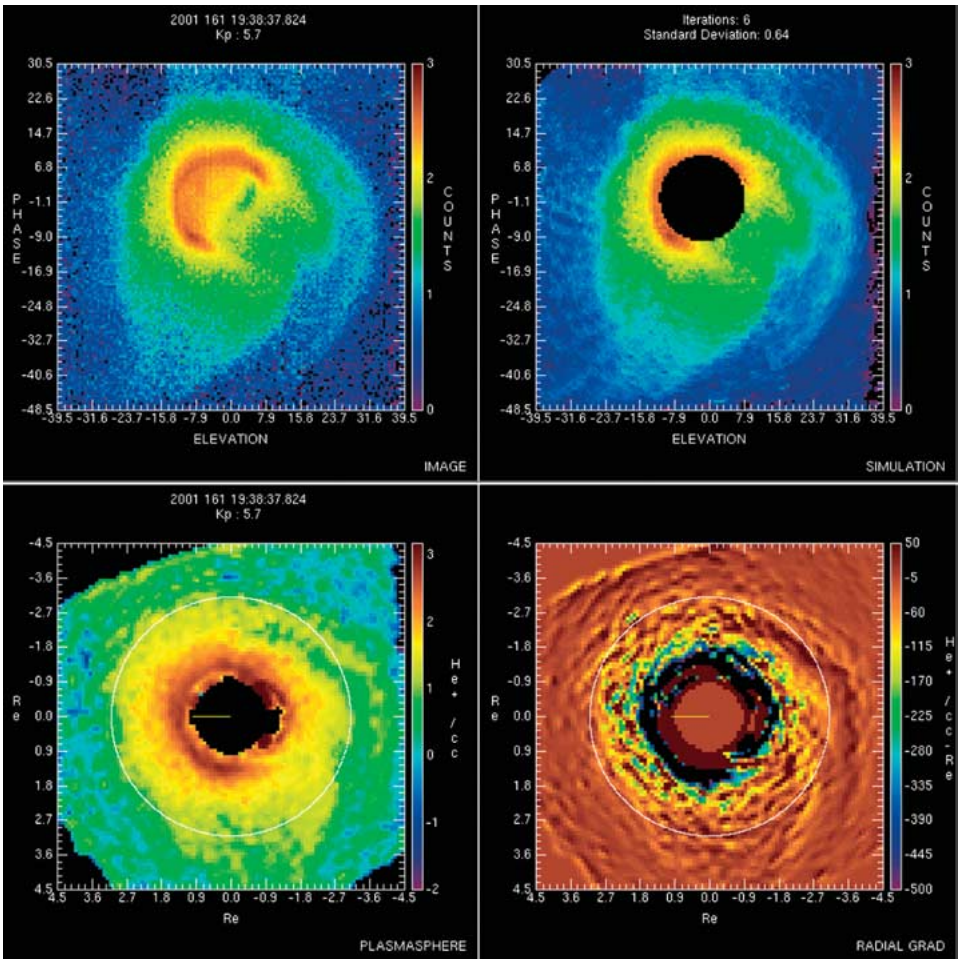

Figure 12. Example of the iterative image inversion, for an EUV image at 2001-161/19:38. (Upper left) The measured EUV image. (Upper right) Resulting simulated image. Both have units of counts sec^{-1}. (Lower left) The He^{+} density in the plane of the geomagnetic equator deduced from the inversion, in ions cm^{-3}. The coordinate system is Solar-Magnetic with the Sun to the left and dusk downward. (Lower right) The radial gradient of the He^{+} density in units of $cm^{-3}R_E^{-1}$.

are not sufficiently similar, a new density solution matrix is built by modifying each base value by the ratio of the corresponding pixels in the measured and simulated images. The iteration then proceeds to convergence.

Figure 12 shows a suite of output images for a single inversion. The time for the inversion, 2001-161/19:38, falls between the second and third intervals illustrating channel formation in Figure 6. At this time the plasmasphere was highly structured, and the detailed agreement between the simulated and real images demonstrates that this inversion technique can reconstruct small details with good fidelity. The

assumption that the density is constant along a flux tube is probably less valid at $L < 2$, so the densities deduced there are uncertain.

12. Summary and Conclusions

EUV imaging of the plasmasphere has improved our understanding of the distribution of plasma in the inner magnetosphere and the forces that control it. In addition to their intrinsic interest, the images are useful for establishing the global context that can enhance the interpretation of past and contemporaneous *in situ* measurements.

Acknowledgements

We thank especially Don Carpenter for his insight and encouragement in all phases of this work. We thank Mark Adrian, Alex Dessler, Randy Gladstone, James Green, Patricia Reiff, and Richard Wolf for their contributions. We thank Chris Gurgiolo for allowing us to publish the results of his image deconvolution work. We thank J. L. Burch, the IMAGE Mission Principal Investigator, for his untiring efforts that have made the mission a success. The IMAGE mission has been ably supported by the Mission Operations team at GSFC, under the direction of Richard Burley. Work at Rice University and at The University of Arizona was funded by subcontracts to those institutions from Southwest Research Institute, under NASA contract NAS5-96020 with SwRI. Additional work at Rice University was supported by NASA's Sun-Earth-Connections Theory program under grant ATM NAG5-11881.

References

Brice, N.M.: 1967, 'Bulk motion of the magnetosphere', *J. Geophys. Res.* **72**, 5193.

Burch, J.L. *et al.*: 2001a, 'Views of the Earth's magnetosphere with the IMAGE satellite', *Science* **291**, 619.

Burch, J.L., Mitchell, D.G., Sandel, B.R., Brandt, P.C:son, and Wüest, M.: 2001b, 'Global dynamics of the plasmasphere and ring current during magnetic storms', *Geophys. Res. Lett.* **28**, 1159–1162.

Carpenter, D.L., and Park, C.G.: 1973, 'What ionospheric workers should know about the plasmapause/plasmasphere', *Rev. Geophys.* **11**, 133–154.

Carpenter, D.L., Smith, A.J., Giles, B.L., Chappell, C.R., and Decreau, P.M.E.: 1992, 'A case study of plasma in the dusk sector associated with enhanced magnetospheric convection', *J. Geophys. Res.* **97**, 1157.

Carpenter, D.L., Anderson, R.R., Calvert, W., and Moldwin, M.B.: 2000, 'CRRES observations of density cavities inside the plasmaphere', *J. Geophys. Res.* **105**, 23,323–23,338.

Fok, M.-C., Kozyra, J.U., Nagy, A.F., and Cravens, T.E.: 1991, 'Lifetime of ring current particles due to coulomb collisions in the plasmasphere', *J. Geophys. Res.* **96**, 7861.

Foster, J.C., Erickson, P.J., Coster, A.J., Goldstein, J., and Rich, F.J.: 2002, 'Ionospheric signatures of plasmaspheric tails', *Geophys. Res. Lett.* 10.1029/2002GL015067.

Freeman, J.W.: 1993, 'Magnetospheric Specification Model development code and documentation. Report for USAF contract F19628-90-K-0012', Rice University, Houston, TX.

Gallagher, D.L., Craven, P.D., and Comfort, R.H.: 2000, 'Global core plasma model', *J. Geophys. Res.* **105**, 18819.

Garcia, L.N., Fung, S.F., Green, J.L., Boardsen, S., Sandel, B.R., and Reinisch, B.W.: 2002, 'Comparisons of IMAGE RPI and EUV observations of plasma density structures outside of the plasmasphere', *J. Geophys. Res.*, in press.

Goldstein, J., Spasojevic, M., Reiff, P.H., Sandel, B.R., Forrester, W.T., Gallagher, D.L., and Reinisch, B.W.: 2002a, 'Identifying the Plasmapause in IMAGE EUV data using IMAGE RPI *in situ* steep density gradients', *J. Geophys. Res.* **108**, 10.1029/2002JA009475.

Goldstein, J., Spiro, R.W., Reiff, P.H., Wolf, R.A., Sandel, B.R., Freeman, J.W., and Lambour, R.L.: 2002b, 'IMF-driven overshielding electric field and the origin of the plasmaspheric shoulder of May 24, 2000', *Geophys. Res. Lett.* 10.1029/2001GL014534.

Goldstein, J., Sandel, B.R., Forrester, W.T., and Reiff, P.H.: 2002c, 'IMF-driven plasmasphere erosion of 10 July 2000', *Geophys. Res. Lett.* **30**, 10.1029/2002GL016478.

Grebowsky, J.M.: 1970, 'Model study of plasmapause motion', *J. Geophys. Res.* **75**, 4329.

Green, J.L., and Reinisch, B.W.: 2002, 'An Overview of results from RPI on IMAGE', *Space Science Reviews*, this issue.

Green, J.L., Sandel, B.R., Fung, S.F., Gallagher, D.L., and Reinisch, B.W.: 2002, 'On the origin of kilometric continuum', *J. Geophys. Res.* 10.1029/2001JA000193.

Gurgiolo, C., Sandel, B., and Gallagher, D.: 2000, 'First attempt at producing a 3d plasmasphere model from EUV images', Magnetospheric Imaging Workshop, Yosemite Nat'l Park, CA, 5–8 Feb.

Hashimoto, K.W., Calvert, W., and Matsumoto, H.: 1999, 'Kilometric continuum detected by GEOTAIL', *J. Geophys. Res.* **104**, 28645–28656.

Horwitz, J.L., Comfort, R.H., and Chappell, C.R.: 1990, 'A statistical characterization of the plasmasphere density structure and boundary locations', *J. Geophys. Res.* **95**, 7937–7947.

Jaggi, R.K., and Wolf, R.A.: 1973, 'Self-consistent calculation of the motion of a sheet of ions in the magnetosphere', *J. Geophys. Res.* **78**, 2852.

Jordanova, V.K., Kozyra, J.U., Nagy, A.F., and Khazanov, G.V.: 1997, 'Kinetic model of the ring current-atmosphere interactions', *J. Geophys. Res.* **102**, 14,279.

Kozyra, J.U., Jordanova, V.K., Horne, R.B., and Thorne, R.M.: 1997, 'Modeling of the contribution of electromagnetic ion cyclotron (EMIC) waves to stormtime ring current erosion', in B.T. Tsurutani (ed.), *Magnetic Storms*, p. 187, AGU, Washington DC.

Moldwin, M., Sandel, B., Thomsen, M, and Elphic, R.: 2002, 'Quantifying global plasmaspheric images with *in situ* observations', *Space Science Reviews*, this issue.

Nishida, A.: 1966, 'Formation of plasmapause, or magnetospheric plasma knee, by the combined action of magnetospheric convection and plasma escape from the tail', *J. Geophys. Res.* **71**, 5669.

Roelof, E.C., and Skinner, A.J.: 2000, 'Extraction of ion distributions from magnetospheric ENA and EUV images', *Space Sci. Rev.* **91**, 437.

Sandel, B.R., Broadfoot, A.L., Curtis, C.C., King, R.A., Stone, T.C., Hill, R.H., Chen, J., Siegmund, O.H.W., Raffanti, R., Allred, D.D., Turley, R.S., and Gallagher, D.L.: 2000, 'The extreme ultraviolet imager investigation for the IMAGE mission', *Space Science Reviews* **91**, 197–242.

Sandel, B.R., King, R.A., Forrester, W.T., Gallagher, D.L., Broadfoot, A.L., and Curtis, C.C.: 2001, 'Initial results from the IMAGE extreme ultraviolet imager', *Geophys. Res. Lett.* **28**, 1439–1442.

Wolf, R.A., *et al.*: 1997, 'Modeling convection effects in magnetic storms', *in* B.T. Tsurutani (ed.), *Magnetic Storms*, p. 161, AGU, Washington DC.